Fachbereich 13 Physik
Institut für Theoretische Physik,
Goethe-Universität Frankfurt am Main

Bachelor Thesis

Computation of masses of heavy hybrid mesons from hybrid static potentials

Carolin Riehl

Frankfurt am Main
14. September 2017

Supervisor: Prof. Dr. Marc Wagner
Second supervisor: Prof. Dr. Owe Philipsen

Abstract

In this work, masses of heavy hybrid mesons are calculated from hybrid static potentials. For this purpose, a parametrisation is fitted to lattice data for the hybrid static potentials Π_u and Σ_u^-. Applying the Born-Oppenheimer approximation, a Schrödinger equation for the heavy quark-antiquark pair is derived. By using the fitted hybrid static potential as an input in the Schrödinger equation, binding energies for a system of two bottom quarks are computed numerically. From this, we obtain heavy hybrid meson masses and discuss corresponding meson quantum numbers.

Zusammenfassung

In dieser Arbeit werden Massen für schwere hybride Mesonen aus statischen hybriden Potentialen berechnet. Dafür werden die Parameter einer analytischen Potentialfunktion durch Fits an Gitterdaten für die statischen hybriden Potentiale Π_u und Σ_u^- bestimmt. In der Born-Oppenheimer-Näherung wird die Schrödingergleichung für das schwere Quark-Antiquark-Paar hergeleitet. Das Spektrum für Bottom-Quarks in einem statischen hybriden Potential wird numerisch aus der Schrödingergleichung berechnet. Daraus erhalten wir Massen für schwere hybride Mesonen und ordnen sie möglichen Mesonen-Quantenzahlen zu.

Contents

1 Introduction

1.1 Motivation

Quantum Chromodynamics (QCD) describes the strong interaction in theoretical physics. The strong interaction belongs to the fundamental forces of nature. It is mediated by gluons, the gauge bosons of QCD, which is a non-abelian gauge theory of the SU(3)-color gauge group. Due to the large coupling constant of QCD at low energies, a perturbative treatment of the theory is not possible in the region of small energies or large distances. Therefore, lattice QCD is used which evaluates physical quantities on a discretized spacetime, the lattice. Here, a numerical treatment is possible.

Mesons are systems bound by the strong interaction. In the quark model, they consist of a quark and an antiquark. Beyond that, the gluonic field causing the binding of quark and antiquark can be excited, it then contributes to the quantum numbers of the meson. Such bound states with exotic quantum numbers that cannot be explained by the simple quark model are called *hybrid mesons*. An example for an exotic quantum number state is the $J^{PC} = 1^{-+}$ state for which two candidates, the $\pi_1(1400)$ and the $\pi_1(1600)$ states, were measured in experiments. An alternative way of explaining these states are exotic quark structures like tetraquarks. Exotic mesons are an important topic for the understanding of the strong interaction. Studying such states theoretically can give predictions for hadron spectroscopy and experiments like PANDA at FAIR searching for glueballs and hybrid mesons.

The aim of this work is to compute masses of hybrid mesons with heavy bottom quarks by inserting hybrid static potentials into the Schrödinger equation. This was previously done for the ground state static potential finding the bottomonium spectrum [1]. Similarly, we develop methods to fit the hybrid static potential data that was calculated in [2]. Furthermore, an approach is described to arrive at a Schrödinger equation for the heavy quarks in a hybrid static potential caused by the gluons. We explain how to obtain masses of heavy hybrid mesons from numerical methods. In this work, masses are calculated from the hybrid static potentials Π_u and Σ_u^- for a bottom and antibottom quark pair and assigned to possible meson quantum numbers.

1.2 Theory

Discretizing spacetime with a lattice enables a numerical treatment of QCD using statistical methods. Path integrals can be solved on the lattice by using Monte-Carlo simulations that generate a large number of field configurations with the corresponding weight factor of the path integral $\propto \frac{e^{-S}}{Z}$, where S is the QCD action and Z denotes a normalization factor. The path integral expression is calculated by averaging over these field configurations. After defining operators $\mathcal{O}$ that create a trial state from the vacuum with the same quantum numbers as the state of interest, a second step to determine the desired observables is to calculate the corresponding correlation functions. These can be expressed through path integrals as follows

$$C(t) = \left\langle \Omega | \mathcal{O}^\dagger(t)\mathcal{O}(0)|\Omega \right\rangle \tag{1.1}$$

$$= \frac{1}{Z}\int DAD\bar{q}Dq\ \mathcal{O}^\dagger(t)\mathcal{O}(0)e^{-S(A,q,\bar{q})}. \tag{1.2}$$

Here, the integration runs over all possible gauge field and quark field configurations. The operators create a quark and antiquark with a separation r from the vacuum. The quarks are considered to be infinitely heavy and fixed on one lattice site, thus they are static and can be integrated out. Using the euclidian time evolution $\mathcal{O}(t) = e^{Ht}\mathcal{O}(0)e^{-Ht}$ and a set of energy eigenstates to the Hamilton operator and, in the end, taking the limit $t \to \infty$, Equation (1.1) can be modified to:

$$\lim_{t\to\infty} C(t) = \lim_{t\to\infty} \sum_n \langle\Omega|e^{Ht}\mathcal{O}(0)e^{-Ht}|n\rangle \langle n|\mathcal{O}(0)|\Omega\rangle \tag{1.3}$$

$$= \lim_{t\to\infty} \sum_n |\langle n|\mathcal{O}(0)|\Omega\rangle|^2 e^{-(E_n - E_\Omega)t} \tag{1.4}$$

$$\propto e^{-(E_0 - E_\Omega)t}. \tag{1.5}$$

The sum over n runs over all energy eigenstates with the same quantum numbers as the trial state. For large t, the higher energy levels are suppressed so that only the trial state with the lowest energy with $n = 0$ survives. The energy difference $E_0 - E_\Omega$ is defined as the potential $V(r)$ between the quark and the antiquark that can be extracted by fitting an exponential function to the correlator at large t. Another common approach is to fit a constant to the effective potential defined through

$$V_{\text{eff}}(t) = \frac{1}{a}\ln\left(\frac{C(t)}{C(t+a)}\right), \tag{1.6}$$

at large t. Here, a denotes the lattice spacing. To obtain a static potential, one has to use lattice expressions for the correlator. It can be shown that the expectation value of a *Wilson loop*, which is defined as a product of spatial and temporal links along a closed path on the lattice, behaves in the same way as the correlator. Hence, one calculates Wilson loops for each quark separation to obtain static potentials. By varying the shape of spatial paths, the quantum numbers for the static potential can be chosen. Straight paths of links between the two static quarks result in the ground state static potential, whereas more complex insertions within the quark separation produce hybrid static potentials. A hybrid static potential is characterized by the quantum numbers Λ^ϵ_η :

- $\Lambda = 0, \pm1, \pm2, ... = \Sigma, \Pi, \Delta, ...$ denotes the angular momentum with respect to the separation axis of two quarks.
- $\eta = u, g$ stands for the behavior under combination of charge conjugation and parity, $P \circ C = -, +$.
- Only states with $\Lambda = 0$ are nondegenerate with respect to the spatial inversion along the axis perpendicular to the separation axis, P_x, and are designated with an additional quantum number $\epsilon = +, -$.

The Sommer parameter r_0, which is defined through the force $F(r)$ between two static quarks in the ground state static potential

$$F(r_0)r_0^2 = 1.65, \tag{1.7}$$

corresponds to $r_0 \approx 0.5$ fm. The lattice spacing a can be determined by finding the parameters V_0, α and σ of the parametrisation for the ground state static potential

$$V(r) = V_0 - \frac{\alpha}{r} + \sigma r, \tag{1.8}$$

that it is finally determined to be $a = 0.093$ fm for the data used in this work. The methods to obtain the lattice data were developed in [2] where further details can be found.

1.2.1 Jackknife analysis

In the following work, we use the common jackknife analysis to give an estimate of the statistical error. For this purpose, the method is described here. The lattice simulations for the calculation of static potentials provide data sets consisting of a large number of configurations. In this work, we perform the analysis with $N = 700$ configurations. Using the jackknife method, we take into account the correlation of the simulated data [3]. Instead of calculating the standard error of the full sample, reduced samples are constructed by leaving out one of the N configurations. Hence, we obtain N reduced samples consisting of $N-1$ configurations, whereby the standard means are calculated by making use of the formula

$$\tilde{\theta}_i = \frac{1}{N-1} \sum_{k \neq i} x_k. \tag{1.9}$$

The regarded parameters are calculated on the results of each reduced sample. The mean of the full sample is given by

$$\bar{\theta} = \frac{1}{N} \sum_{i=1}^{N} \theta_i. \tag{1.10}$$

Finally, the jackknife error for the estimator of interest is given by

$$\Delta\theta = \sqrt{\frac{N-1}{N} \sum_{i=1}^{N} \left(\tilde{\theta}_i - \bar{\theta}\right)^2}. \tag{1.11}$$

1.3 Outline

In the following the structure of the thesis is outlined. Given the lattice data for hybrid static potentials, fit procedures for the potentials are explained in Chapter 2 to gain a continuous form of the potentials. The next chapter describes the derivation and numerical implementation of the Schrödinger equation for heavy quarks in a hybrid potential. Finally, in Chapter 4 quantum number multiplets for hybrid mesons are deduced and associated to the calculated spectrum of heavy hybrid mesons. Results are presented and discussed.

2 Fitting procedure for the lattice potential

2.1 Parametrisation

To be able to solve the Schrödinger equation, we require continuous functions for the lattice potential data of the Π_u- and Σ_u^--potential that are shown in Figure 2.1. The ground state static potential is mostly fitted with the Cornell potential

$$V(r) = V_0 - \frac{\alpha}{r} + \sigma r. \tag{2.1}$$

The confining nature of strong interaction between two quarks is delineated by a linear term in r for large separations. It is proportional to the string tension σ which is the energy per length of the flux tube between two quarks, the parametrisation also includes corrections to the linear behavior.

A parametrisation for hybrid potentials can be derived in an effective theory, called weakly-coupled potential non-relativistic QCD (pNRQCD). It is explained in detail in [4]. This theory is valid for short quark-antiquark distances, as long as $r \ll 1/\Lambda_{QCD} \approx 0.6$ fm. By multipole expansion, the leading order of the hybrid static energy is given by a r-dependent potential $V(r)$ plus a constant. Using perturbation theory, the potential term turns out to be proportional to $\propto 1/r$. The next-to-leading order correction gives a term quadratic in the quark-antiquark distance. This approach results in the following three-parameter-function

$$V(r) = c_1 + \frac{c_2}{r} + c_3 r^2. \tag{2.2}$$

As distinguished from the phenomenological Cornell potential, this parametrisation includes a quadratic term in r. The absolute value of the energy constant c_1 is physically not relevant.

Other suggestions are to fit only the lowest lying potential Π_u to Equation (2.2) and apply Equation (2.3) to the potential difference to the Π_u-potential [5]

$$\Delta V(r) = c_4 \frac{r^2}{1 + c_5 r^2}. \tag{2.3}$$

It is expected that the candidates for a parametrisation reviewed before are only valid for quark-antiquark separations smaller than 1 fm. Therefore, the large r-region requires another parametrisation

$$V(r) = c_6 r \sqrt{1 + \frac{c_7}{c_6 r^2}}, \quad r > 1 \text{ fm}. \tag{2.4}$$

The function given by Equation (2.4) is motivated by the fine structure of the string picture of QCD exhibiting a linear dependence on the quark-antiquark distance and corrections to this behavior. Therefore, the parameter c_6 represents the string tension σ and c_7 corresponds to

$$c_7 = \frac{\pi(12N - 1)}{6}.$$

For the Π_u-potential the excitation number is $N = 1$, for Σ_u^--excitation $N = 3$ [5]. Applying the formula to the lattice data could serve as a test if either c_6 or c_7 correspond to the expected values. Using different fits for large and small separations would require a continuation between the regions to receive a continuous function that can be inserted in the Schrödinger

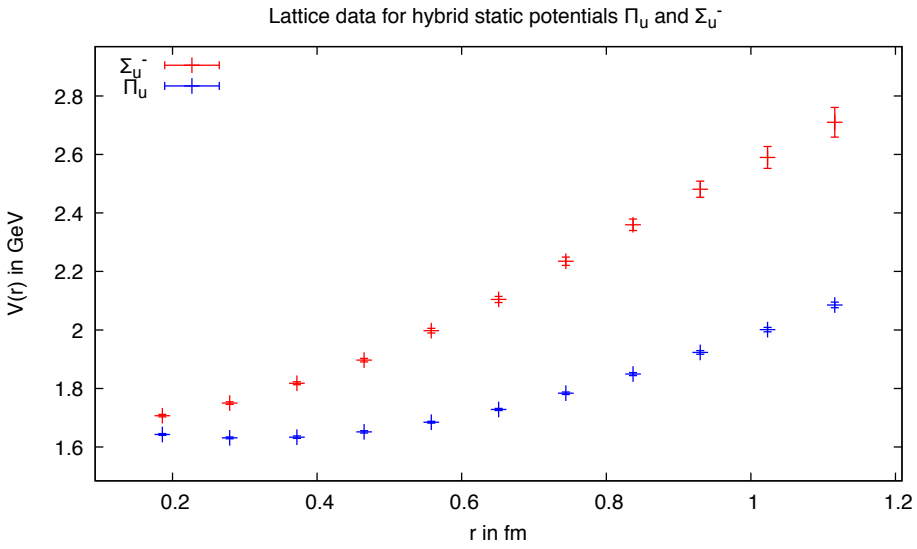

Figure 2.1: Lattice potential data for the Π_u (blue) - and Σ_u^- (red) -potential [2].

equation. Therefore, methods developed in [1] could be used. In the following, the method of least-squares fitting is introduced before results for the fit parameters are discussed.

2.2 Weighted Least-Squares Fitting

Given a set of data points y_i, $i = 1, 2, ..., N$, the parameters c_j, $j = 1, 2..., M$ of a function $f(x_i, c_j)$, that is fitted to the data points, can be found by minimizing the weighted sum of squared residuals

$$\chi^2(c_j) = \sum_{i=1}^{N} \left(\frac{y_i - f(x_i, c_j)}{\sigma_i} \right)^2 . \tag{2.5}$$

The more the fit function suits to the data points, the smaller the value of χ^2 becomes. Since the error of the data points σ_i is included here, points with small error have more weight for the determination of the fit parameters c_j than data with large uncertainties. The value of χ^2 divided by the degrees of freedom, $d.o.f. = N - M$, serves as a criterion for the quality of the fit. An evidence for a proper fit is a value of approximately one. If $\chi^2/d.o.f \gg 1$, the fit model may be improper to describe the data and $\chi^2/d.o.f \ll 1$ occurrs due to correlated fit parameters.

Numerically, the implemented code for a function depending linearly on the fit parameters differs from the one used to solve the minimization problem for non-linear functions. A linear function in c_j can be expressed through

$$f(x_i, \vec{c}) = \sum_{j=1}^{M} A_{ij} c_j, \tag{2.6}$$

where A_{ij} forms the matrix element of a matrix A so that Equation (2.5) becomes

$$\chi^2(c_j) = \sum_{i=1}^{N} \left(\frac{\sum_{j=1}^{M} A_{ij} c_j - y_i}{\sigma_i} \right) \left(\frac{\sum_{l=1}^{M} A_{il} c_l - y_i}{\sigma_i} \right) . \tag{2.7}$$

The weight factors form the diagonal elements of a matrix $W = diag(1/\sigma_1^2, ..., 1/\sigma_N)$. Thus,

parametrisation	$[r_{min}, r_{max}]$	parameters	$\chi^2/d.o.f.$
Equation (2.2)	[0.186 fm, 1.116 fm]	$c_1 = (7.63 \pm 0.03)\frac{1}{\text{fm}}$ $c_2 = 0.118 \pm 0.007$ $c_3 = (2.28 \pm 0.05)\frac{1}{\text{fm}^3}$	0.77
Equation (2.4)	[0.558 fm, 1.116 fm]	$c_6 = (6.39 \pm 0.06)\frac{1}{\text{fm}^2}$ $c_7 = 9.3 \pm 0.2$	1.19

Table 2.1: Fit parameters for two diffferent parametrisations for the Π_u-potential.

minimizing χ^2 is equivalent to solving a linear system of equations $A^T W A\vec{c} - A^T W\vec{y} = 0$. This is performed using Gaussian elimination with back substitution. The errors of the found parameters c_j are computed with a jackknife analysis.

To fit a function that depends non-linearly on the parameters c_j to data points, a program is implemented using GNU Scientific Library (GSL) [6]. GSL uses trust region methods to minimize Equation (2.5) by approximating it with a second order Taylor series expansion around c_j and minimizing this only in a small region. This trust region subproblem is solved for a trial step, evaluated if the objective function is minimized and then the trust region is expanded until it converges finally. Therefore, a Levenberg-Marquardt algorithm is used. The starting point for the parameters has to be in the region of the minimum of Equation (2.5) since the above described methods are local ones. The errors in the parameters for non-linear least square fitting are computed analogous to the case of linear fitting.

2.3 Results

In the following, the fit parameters found by applying the above-described methods to the given lattice potential data points are discussed. The afore-mentioned parametrisations are fitted to lattice data in a dimensionless form. The dimensionfull parameters c_j are obtained from the numerical results $\hat{c}_j$ by using the following relations

$$\begin{aligned} c_1 &= \hat{c}_1/a, & c_2 &= \hat{c}_2, & c_3 &= \hat{c}_3/a^3, \\ c_4 &= \hat{c}_4/a^3, & c_5 &= \hat{c}_5/a^2, & & \\ c_6 &= \hat{c}_6/a^2, & c_7 &= \hat{c}_7, & & \end{aligned} \tag{2.8}$$

where $a = 0.093$ fm is the lattice spacing.

2.3.1 Π_u-potential

First, the parametrisation of Equation (2.2) is fitted to the data of the Π_u-potential. The range of lattice data included in the fit is varied. All fit regions produce acceptable values of reduced $\chi^2 \approx 1$, accordingly, we can use the fit parameters for the whole region in which potential data points are available. The fit function with an errorband for the parameters given in the first row of Table 2.1 is shown in Figure 2.2a. The width of the errorband compared to the errors of the data points is caused by the fact that the parameters of the fitfunction (2.2) are not independent. A change in c_3 causes an adjustment of c_2 to balance the deviation. As only one parameter is varied to plot the errorband, the compensation is not revealed and the band exceeds the data errors. The parameter c_2 is in agreement to the result found in [7] by fitting the same parametrisation to lattice data from [8].

As mentioned before, we can also apply the large r-formula (2.4) to the lattice data. The formula is valid for separation larger than 1 fm for which we have only two points available. Applying the formula in a region between 0.558 fm and 1.116 fm results in the parameters

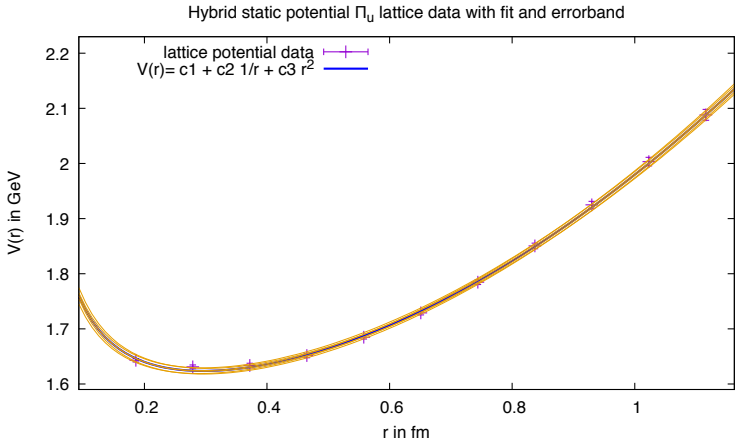

(a) Lattice potential data of the Π_u-potential with fit (2.2) in the region $[0.186\text{ fm}, 1.116\text{ fm}]$ and errorband.

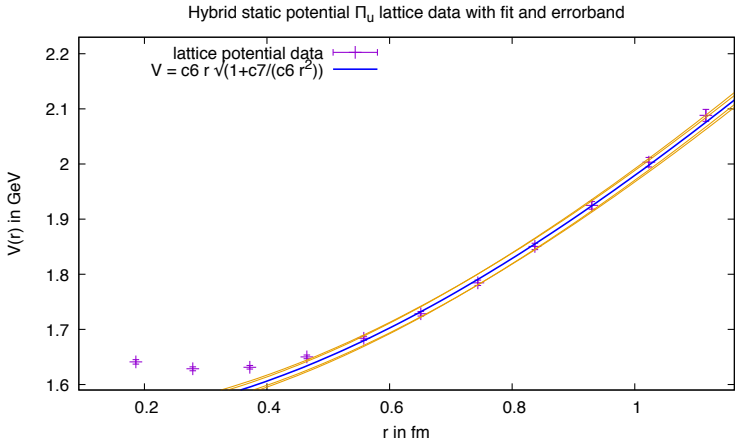

(b) Lattice potential data of the Π_u-potential with fit (2.4) in the region $[0.558\text{ fm}, 1.116\text{ fm}]$ and errorband.

Figure 2.2: Fits for the Π_u-potential.

given in the second row of Table 2.1. The fit is shown in Figure 2.2b. The discrepancies of the parameters to the expected values, such as to the string tension $\sigma \approx 5.4 \pm 0.5 \frac{1}{\text{fm}^2}$, reveal that the parametrisation is improper for the available lattice data to extract the value for the string tension or the parameter c_7. The larger the lower boundary of the fit region, the smaller is the number of data points. Since neighbouring points are correlated, the value of reduced χ^2 gets smaller for less data points, $\chi^2/\text{d.o.f} \ll 1$. The correlation of the parameters can again be seen in the width of the errorband compared to the errors of the data points in Figure 2.2b. To be able to perform better fits with Equation 2.4, we would either need more lattice data for larger separations or fix the string tension parameter to the expected value from the ground state potential fit [5].

For simplicity, we use the fit function of Equation (2.2) with its parameters presented in Table 2.1 for the Π_u-potential to insert it into the Schrödinger equation in the following. It still provides a good fit for the whole region despite the fact that it exceeds the limit to which the parametrisation was derived according to [4].

2.3.2 Σ_u^--potential

A selection of parameters for each parametrisation fitted to the Σ_u^--potential is presented in Table 2.2. Figure 2.3a shows the fit of the Σ_u^--potential with function (2.2) for the whole

parametrisation	$[r_{min}, r_{max}]$	parameters	$\chi^2/d.o.f.$
Equation (2.2)	[0.186 fm, 1.116 fm]	$c_1 = (8.71 \pm 0.07)\frac{1}{\text{fm}}$ $c_2 = -0.04 \pm 0.01$ $c_3 = (4.6 \pm 0.2)\frac{1}{\text{fm}^3}$	2.82
Equation (2.4)	[0.558 fm, 1.116 fm]	$c_6 = (10.0 \pm 0.2)\frac{1}{\text{fm}^2}$ $c_7 = 7.2 \pm 0.3$	0.57
Equation (2.3)	[0.186 fm, 1.116 fm]	$c_4 = (8.5 \pm 0.3)\frac{1}{\text{fm}^3}$ $c_5 = (2.0 \pm 0.2)\frac{1}{\text{fm}^2}$	1.16

Table 2.2: Fit parameters for different parametrisations for the Σ_u^--potential.

range of available lattice data points. The fact that, reducing the upper boundary for the fit region, the parameter c_2 changes its sign and has large uncertainties and the high value of reduced χ^2 as well, reveal that the parametrisation is not optimal for the Σ_u^--potential in the whole region. To obtain physically meaningful values for the parameter c_2, data points for smaller separations need to be added as the term $\propto \frac{1}{r}$ becomes dominant in this region.

Better fits are achieved by applying the fit function (2.3) to the potential difference to the Π_u-potential as can be seen in Figure 2.3b. The disadvantage of this fit function is that the lower lying potential has to be added again to obtain a potential function that can be inserted into the Schrödinger equation. This would increase the errors of the fit.

Similar to the case of the Π_u-potential, the fit function (2.4) for large quark-antiquark separations is fitted to the lattice data in a region between [0.558 fm, 1.116 fm]. The plot can be found in Figure 2.3c with the parameters listed in Table 2.2. For the deviation of the found parameters to the expected values, the same arguments hold as for the Π_u-potential. As before, we need either more data in the large r-region or fix one parameter by a known value to improve the quality of the fit.

In the following, we use the parametrisation of Equation (2.2) with the parameters from Table 2.2 due to the fact that it can be directly inserted into the Schrödinger equation.

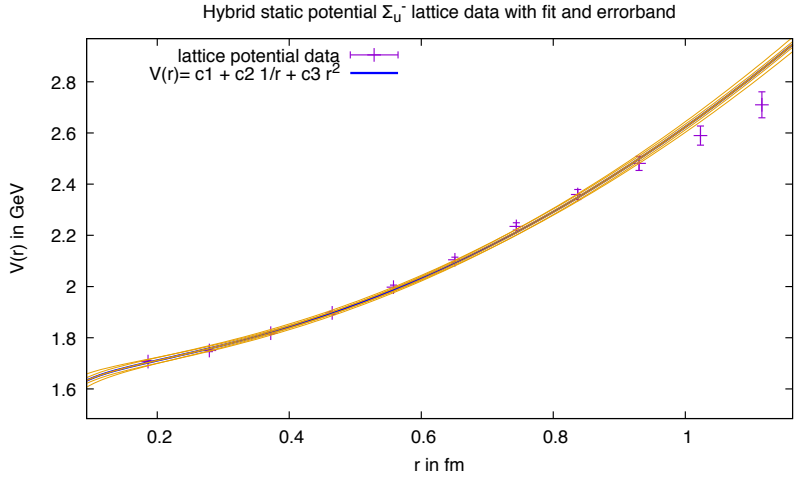

(a) Lattice potential data of the Σ_u^--potential with fit (2.2) in the region $[0.186\text{ fm}, 1.116\text{ fm}]$ and errorband.

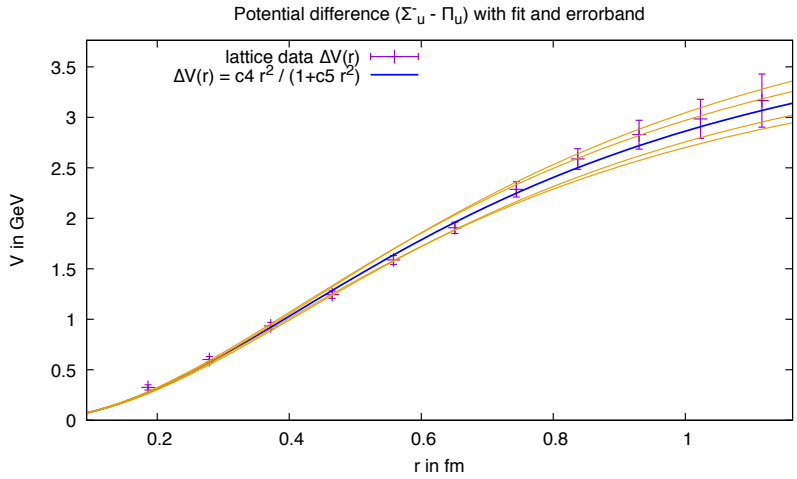

(b) Potential difference between lattice data of the Π_u- and Σ_u-potential with fit (2.3) in the region $[0.186\text{ fm}, 1.116\text{ fm}]$ and errorband.

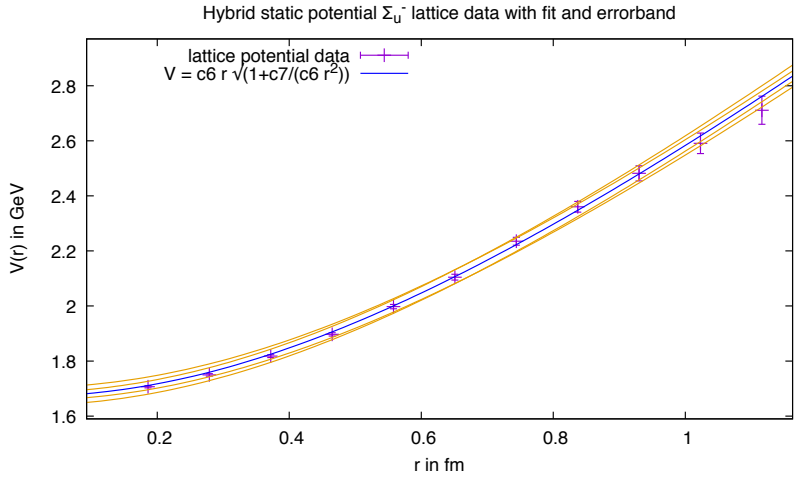

(c) Lattice potential data of the Σ_u^--potential with fit (2.4) in the region $[0.558\text{ fm}, 1.116\text{ fm}]$ and errorband.

Figure 2.3: Fits for the Σ_u^--potential.

3 Solving the Schrödinger equation

3.1 Derivation

The spectrum of hybrid mesons is determined by solving

$$\hat{H}\,|\psi\rangle = E\,|\psi\rangle \tag{3.1}$$

for its energy eigenvalues. Since it is very difficult to compute heavy hybrid meson masses using lattice QCD with quarks of finite mass, one can choose the *Born-Oppenheimer approximation* as first proposed in [9]. For further details see [5] and [10]. With this approximation, the computation is reduced to solving a Schrödinger equation for the heavy quark-antiquark pair in a potential generated by the gluons. This is explained in the following.

In the case of diatomic molecules, the Born-Oppenheimer approximation enables the calculation of molecular energy levels by solving the Schrödinger equation. It provides an equation for the heavy nuclei in a potential generated by the light degrees of freedom, the electrons, at fixed nuclei positions. It is rooted in the existence of slow and fast degress of freedom, two types of particles with masses differing in orders of magnitude and therefore with different time scales. The Born-Oppenheimer approximation consists of the *adiabatic approximation* stating that the light degrees of freedom adapt to changes of the heavy nuclei while remaining in the instantaneous eigenstate. This approximation exploits the fact of two different time scales. Subsequently, the *single-channel approximation* neglects contributions of mixing between states from different stationary electronic eigenstates. Hybrid mesons exhibit the same characteristics as diatomic molecules, consequently the Born-Oppenheimer approximation can be applied to our problem.

The first step is to calculate the potentials generated by the light degrees of freedom using lattice QCD with static sources as quarks. This was performed in [2]. This work deals with the second step which is the solution of the Schrödinger equation for heavy quarks in a hybrid static potential.

The Hamilton operator describing the dynamics of heavy hybrid mesons can be divided into the sum of the gluonic Hamilton operator and the kinetic energy of the quark-antiquark pair

$$\mathbf{H}(\vec{r}) = \mathbf{H}_{gluon}(\vec{r}) + \mathbf{T}_{q\bar{q}}(\vec{r}). \tag{3.2}$$

The former is given by the QCD Hamiltonian describing the dynamics of the gluon field. It also includes the interaction between gluon field and static quarks. The Hamilton operator depends on the relative coordinate of the two quarks $\vec{r}$. The center of mass coordinates can be integrated out since they are not relevant for the spectrum of heavy hybrid mesons. The kinetic energy of the quark-antiquark pair is

$$\mathbf{T}_{q\bar{q}} = \frac{-1}{2\mu}\Delta = \frac{-1}{2\mu}\left(\frac{1}{r^2}\partial_r\left(r^2\partial_r\right) - \frac{\mathbf{L}_{q\bar{q}}^2}{r^2}\right), \tag{3.3}$$

with $\mathbf{L}_{q\bar{q}}$ being the orbital angular momentum operator and μ denoting the reduced mass of the quark-antiquark pair.

In the first place, considering the static limit with infinitly heavy quarks, the kinetic energy of the quarks can be neglected due to its proportionality to $\propto 1/\mu$ in contrast to the gluonic

energy. The problem (3.1) reduces to

$$\mathbf{H}_{gluon} \left|\psi\right\rangle = E \left|\psi\right\rangle . \tag{3.4}$$

The eigenvalue equation for the gluonic Hamiltonian is given by

$$\mathbf{H}_{gluon} \left|m; \vec{r}\right\rangle = V_m(r) \left|m; \vec{r}\right\rangle , \tag{3.5}$$

where the eigenvalue $V_m(r)$ is the static potential calculated on the lattice for each quark-antiquark separation r using static sources as quarks. The index m represents the quantum numbers of the corresponding gluonic state. The eigenfunction $|\psi\rangle$ of the full system can be expanded in terms of the eigenstates for the gluonic Hamiltonian

$$\left|\psi\right\rangle = \sum_k \psi_n^{(k)}(\vec{r}) \left|k; \vec{r}\right\rangle . \tag{3.6}$$

Substituting the expansion of eigenstates in the total Equation (3.1), making use of Equation (3.5) and multiplying it with $\langle m; \vec{r}|$ yields

$$\begin{aligned} \left[V_m(r) + \frac{-1}{2\mu r^2}\partial_r \left(r^2 \partial_r\right)\right] \psi_n^{(m)}(\vec{r}) + \frac{1}{2\mu r^2} \sum_k \left\langle m; \vec{r} \left| \mathbf{L}^2_{q\bar{q}} \right| k; \vec{r} \right\rangle \psi_n^{(k)}(\vec{r}) \\ + \{terms \propto \partial_r \left|k; \vec{r}\right\rangle\} \\ = E_n^{(m)} \psi_n^{(m)}(\vec{r}). \end{aligned} \tag{3.7}$$

Since we assume the gluon field to remain in its instantaneous eigenstate when the quark coordinate r changes slowly, which corresponds to the adiabatic approximation, we neglect the radial derivative acting on the gluonic state

$$\partial_r \left|k; \vec{r}\right\rangle \approx 0. \tag{3.8}$$

As a consequence of the adiabatic change, we can assume for the low lying hybrid static potentials that they are separated well enough that the gluon eigenstates do not mix. Therefore, we neglect all contributions but one $\psi_n^{(m)}$ corresponding to a single gluon configuration m. This is equivalent to assuming

$$\left|\psi\right\rangle \approx \psi_n^{(m)}(\vec{r}) \left|m; \vec{r}\right\rangle . \tag{3.9}$$

What remains from the sum in the second term of Equation (3.7) is only the diagonal term

$$\frac{1}{2\mu r^2} \left\langle m; \vec{r} \left| \mathbf{L}^2_{q\bar{q}} \right| m; \vec{r} \right\rangle \psi_n^{(m)}(\vec{r}). \tag{3.10}$$

The wave function can be splitted into a radial and an angular part using

$$\psi_n^{(m)}(\vec{r}) = \frac{u_n(r)}{r}\ Y(\theta, \phi). \tag{3.11}$$

Finally, in the Born-Oppenheimer approximation problem (3.1) results in

$$\left(\frac{-1}{2\mu}\frac{d^2}{dr^2} + \frac{\left\langle \mathbf{L}^2_{q\bar{q}} \right\rangle^{(m)}}{2\mu r^2} + V_m(r) - E_n^{(m)}\right) u_n(r)\ Y(\theta, \phi) = 0. \tag{3.12}$$

To summarize, after evaluating the effect of the orbital angular momentum operator, we arrive at a one-dimensional, non-relativistic Schrödinger equation for the radial quark-antiquark wave function with an effective potential consisting of the hybrid static potential $V_m(r)$ and the centrifugal term.

3.2 Centrifugal term

In this section, two approaches are discussed to evaluate the centrifugal term in Equation (3.12).

Naively, one can start by replacing the angular momentum operator of the quark-antiquark-pair with its eigenvalue $L_{q\bar{q}}(L_{q\bar{q}}+1)$ corresponding to the spherical harmonics, $Y_{Lm}(\theta,\phi)$. A difficulty arises when trying to refer the found eigenstates characterised by the angular momentum of the quark and antiquark to meson quantum numbers. Therefore, one can choose a superior approach reviewed in the following. For details see [5] where this approach has been proposed. A great advantage of it is that we can then associate the quantum numbers of the found eigenstates to the meson quantum numbers as explained in Section 4.1.

The total orbital angular momentum of the hybrid meson is given by the orbital angular momentum of the quark-antiquark pair and the total angular momentum of the gluons

$$\mathbf{L} = \mathbf{L}_{q\bar{q}} + \mathbf{J}_g. \tag{3.13}$$

The square of the angular momentum operator of the quark-antiquark pair is then given by

$$\begin{aligned} \mathbf{L}_{q\bar{q}}^2 &= \mathbf{L}^2 - 2\mathbf{L}\mathbf{J}_g + \mathbf{J}_g^2 && (3.14)\\ &= \mathbf{L}^2 - 2\mathbf{L}_z\mathbf{J}_{gz} + (L_+J_{g,-} + L_-J_{g,+}) + \mathbf{J}_g^2. && (3.15) \end{aligned}$$

The linear combination of ladder operators $L_\pm$ couples the gluonic eigenstates. As we are working in the single channel approximation, this term is neglected in the following. Evaluating the expectation value of the operators gives

$$\begin{aligned} \left\langle \Lambda,\eta,\epsilon;\vec{r}\,\middle|\mathbf{L}^2\middle|\Lambda,\eta,\epsilon;\vec{r}\,\right\rangle \psi_n^{(m)}(\vec{r}) &= L(L+1)\ \psi_n^{(m)}(\vec{r}), && (3.16)\\ \langle \Lambda,\eta,\epsilon;\vec{r}\,|2\mathbf{L}_z\mathbf{J}_{gz}|\Lambda,\eta,\epsilon;\vec{r}\,\rangle \psi_n^{(m)}(\vec{r}) &= 2\Lambda^2\ \psi_n^{(m)}(\vec{r}), && (3.17)\\ \left\langle \Lambda,\eta,\epsilon;\vec{r}\,\middle|\mathbf{J}_g^2\middle|\Lambda,\eta,\epsilon;\vec{r}\,\right\rangle \psi_n^{(m)}(\vec{r}) &= \left\langle \mathbf{J}_g^2\right\rangle^{(m)}\ \psi_n^{(m)}(\vec{r}), && (3.18) \end{aligned}$$

where $|\Lambda,\eta,\epsilon;r\rangle$ represents the gluon configuration with its quantum numbers. In Equation (3.17), it is used that the component of $\mathbf{L}_{q\bar{q}}$ parallel to the separation axis z vanishes by definition. Consequently, the z-component of $\mathbf{L}$ is given by $J_{g,z}=\Lambda$. Inserting this into the Schrödinger equation leads to

$$\left(\frac{-1}{2\mu}\frac{d^2}{dr^2} + \frac{L(L+1)-2\Lambda^2+\left\langle \mathbf{J}_g^2\right\rangle^{(m)}}{2\mu r^2} + V(r)\right) u_{nL} = E_{nL}u_{nL}(r). \tag{3.19}$$

In [5] it is argued that the value of $\left\langle \mathbf{J}_g^2\right\rangle^{(m)}$ should be 2 for the Π_u - and Σ_u^--potentials. According to this work, one justification for the expectation value of the gluon angular momentum operator is given in the constituent gluon picture in which a $J_g=1$-gluon accompanies the quark-antiquark pair. As explained above, the value of the z-component of $\mathbf{L}$ is given by $J_{g,z}=\Lambda$. As a consequence, we obtain a restriction of the orbital angular momentum, namely $L\geq\Lambda$. Therefore, there will be a $L=0$ state for the Σ_u^--potential, but not for Π_u.

In the following we investigate the two cases:

- **A** : A centrifugal term consisting of the orbital angular momentum of the quark-antiquark pair:
$$\frac{L_{q\bar{q}}(L_{q\bar{q}}+1)}{2\mu r^2}. \tag{3.20}$$

The Schrödinger equation then reads

$$\left(\frac{-1}{2\mu}\frac{d^2}{dr^2} + \frac{L_{q\bar{q}}(L_{q\bar{q}}+1)}{2\mu r^2} + V(r)\right) u_{nL_{q\bar{q}}} = E_{nL_{q\bar{q}}} u_{nL_{q\bar{q}}}(r). \tag{3.21}$$

- **B** : A centrifugal term with the total angular momentum of the hybrid meson:

$$\frac{L(L+1) - 2\Lambda^2 + 2}{2\mu r^2}, \quad L \geq \Lambda. \tag{3.22}$$

The Schrödinger equation is given by

$$\left(\frac{-1}{2\mu}\frac{d^2}{dr^2} + \frac{L(L+1) - 2\Lambda^2 + 2}{2\mu r^2} + V(r)\right) u_{nL} = E_{nL} u_{nL}(r). \tag{3.23}$$

Finally, we arrive at an equation that is equivalent to a one-dimensional Schrödinger equation with energy eigenvalues E_{nl} depending on the principal number n and the angular orbital momentum $l = L_{q\bar{q}}$ or L for **A** or **B**, respectively.

3.3 Numerical implementation

To solve the Schrödinger equation numerically, it is convenient to make it dimensionless. Multiplying Equation (3.12) with the lattice spacing a leads to

$$\frac{-a}{2\mu}\frac{d^2 u_{nl}}{dr^2} + \left(V(r)a + \frac{\left\langle \mathbf{L}^2_{q\bar{q}} \right\rangle^{(m)}}{2\mu r^2} a - E^{(m)}_{nl} a\right) u_{nl}(r) = 0. \tag{3.24}$$

Now we can identify the dimensionless quantities:

$$\begin{aligned} \hat{r} &= r a^{-1} \\ \hat{V} &= V a \\ \hat{\mu} &= \mu a \\ \hat{E}^{(m)}_{nl} &= E^{(m)}_{nl} a. \end{aligned} \tag{3.25}$$

The dimensionless Schrödinger equation is

$$\frac{-1}{2\hat{\mu}}\frac{d^2 u_{nl}}{d\hat{r}^2} + \left(\hat{V}(\hat{r}) + \frac{\left\langle \mathbf{L}^2_{q\bar{q}} \right\rangle^{(m)}}{2\hat{\mu}\hat{r}^2} - \hat{E}^{(m)}_{nl}\right) u_{nl}(\hat{r}) = 0, \tag{3.26}$$

with an effective potential

$$\hat{V}_{\text{eff}} = \hat{V}(\hat{r}) + \frac{\left\langle \mathbf{L}^2_{q\bar{q}} \right\rangle^{(m)}}{2\hat{\mu}\hat{r}^2}. \tag{3.27}$$

For numerical treatment, the boundary conditions can be formulated as follows:

$$h(y(\hat{r}_{min})) = \frac{u_{nl}(\hat{r}_{min})}{\hat{r}^{s+1}_{min}} - \frac{u_{nl}(\hat{r}_{min}+\epsilon)}{(\hat{r}_{min}+\epsilon)^{s+1}} = 0 \tag{3.28}$$

$$u_{nl}(\hat{r}_{max}) = 0. \tag{3.29}$$

The value of s is derived in Appendix A where we work out the behavior of the radial probability amplitude for small r in detail.

The Schrödinger equation (3.26), which is an eigenvalue equation, can be rewritten into a

system of first order differential equations

$$\frac{d}{d\hat{r}} \begin{pmatrix} y \\ \frac{dy}{d\hat{r}} \\ E \end{pmatrix} = \begin{pmatrix} u_{nl} \\ 2\hat{\mu}\left[\hat{V} + \frac{1}{2\hat{\mu}\hat{r}^2}\left\langle \mathbf{L}^2_{q\bar{q}} \right\rangle - \hat{E}\right] y_1 \\ 0 \end{pmatrix}, \tag{3.30}$$

that can be solved numerically using standard methods. A shooting method is implemented with a Newton-Raphson method using a fourth order Runge-Kutta algorithm in every step. It starts with initial values for $y, y\prime$ and E, where the boundary condition (3.29) fixes the first one. The second initial value $y\prime$ is arbitrary because it only influences the normalization. The remaining initial value has to be guessed. Now, one "shoots" from $\hat{r}_{max}$ to a minimum separation $\hat{r}_{min}$ and then varies the initial guess for the energy eigenvalue to meet the boundary condition $h(y(\hat{r}_{min}))$. For this purpose, we modify the initial guess E by $dE = -h(y(\hat{r}_{min})) * \frac{1}{\partial_E h(y(\hat{r}_{min}))}$ until dE falls below a chosen criterion E_{min}. The Newton-Raphson method converges only for an initial guess of E close enough to the exact root of the function h.

The idea behind starting the integration at $\hat{r}_{max}$ is to avoid a problem that occurs in a region which is classically forbidden for the wave function. For the wave function in a potential larger than its energy there is an exponentially increasing and a decreasing solution which depends on the size of the energy differences. Physically, only the exponentially decreasing solution is allowed.

If the effective potential (3.27) is many orders larger than the energy eigenvalue, there exists a numerical difficulty in finding a solution without an exponentially increasing part. Hence, the solution to Equation (3.26) for regions of large effective potentials is unstable.

In our case, the effective potential (3.27) becomes large for small r as well as for large r. Therefore, the problem of unstable solutions also occurs when integrating from $\hat{r}_{max}$ to $\hat{r}_{min}$.

Numerically, the described behavior can be avoided by implementing a Runge-Kutta algorithm starting its integration in the classically forbidden region for small r and one integrating from the forbidden large r region. The boundary condition is then called *logarithmic*. At the point, r_m, where both integrations end their values and derivatives should fulfill

$$\frac{u\prime_1(r_m)}{u_1(r_m)} - \frac{u\prime_2(r_m)}{u_2(r_m)} = 0. \tag{3.31}$$

But, since the energy eigenvalue turns out to be stable even if the boundary condition is not fulfilled perfectly, we choose to improve only the termination condition of the Newton-Raphson algorithm. The algorithm of finding the energy eigenvalue is stopped if the Newton step size $|dE| < E_{min}$ and the solution decreases or shows a sign change

$$\begin{aligned} |u(r_{min})| &< |u(r_{min} + \epsilon)| \quad \vee \\ u(r_{min})(E + dE) * u(r_{min})(E) &< 0. \end{aligned} \tag{3.32}$$

3.3.1 Hydrogen atom

The Schrödinger equation for the hydrogen atom can be solved with the same methods and boundary conditions as described above. In comparison to the hybrid static potential, the potential for hydrogen is given by a negative Coulomb term for which the Schrödinger equation can be solved analytically. The energy eigenvalues are proportional to $\propto 1/n^2$ with $n = 1, 2, ...$ Hence, the problem of the hydrogen atom is suitable for a check of our implementation for finding energy eigenvalues for hybrid mesons.

For this purpose, we implement the differential equation

$$\frac{d}{d\hat{r}}\begin{pmatrix} y \\ \frac{dy}{d\hat{r}} \\ E \end{pmatrix} = \begin{pmatrix} u_{nl} \\ \left(\frac{-2}{\hat{r}} + \frac{l(l+1)}{\hat{r}^2} - \hat{E}_n\right) y_1 \\ 0 \end{pmatrix}, \tag{3.33}$$

where $r/a_B = \hat{r}$ and $a_B = \frac{4\pi\hbar^2}{e^2 m_e} \approx 0.529\text{Å}$. To obtain a good initial guess for the energy value to insert in the Newton method, the boundary condition (3.28) is scanned for roots with respect to E. We observe a dependence of the number of found energy eigenvalues on the chosen value of integration boundary r_{max}. The larger the value for r_{max}, the more energy eigenvalues are found. It was checked that the physical quantities do not depend on the remaining numerical parameters like Runge-Kutta step size or the lower integration boundary r_{min}. With the written program, the first three energy eigenvalues can be reproduced for angular momentum $l = 0, 1, 2$.

The above-mentionend problem of unstable solutions for the radial probability amplitude u_{nl} in the presence of large effective potentials can already be seen for the hydrogen atom. In Figure 3.1a the radial probability amplitude is plotted for a corresponding energy eigenvalue and small deviations from it in a negative effective potential. Here, we obtain a stable solution that vanishes for $r \to 0$. In comparison, Figure 3.1b belongs to a solution in a high effective potential for which the radial probability amplitude is unstable with respect to small deviations of the energy eigenvalue. To deal with this problem, we implement the improved termination condition (3.32) mentioned before.

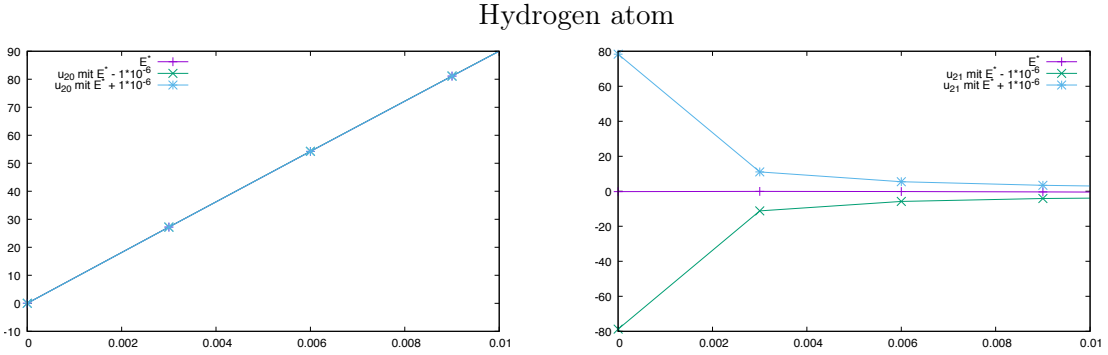

(a) The $1S$ wave function of the hydrogen atom is plotted for the energy eigenvalue $E^* = -0.25$ which was found by the Newton method and for small deviations of $\Delta E = 1 * 10^{-6}$ from this value. The solution is stable.

(b) The $1P$ wave function of the hydrogen atom is plotted for the energy eigenvalue $E^* = -0.25$ which was found by the Newton method and for small deviations of $\Delta E = 1 * 10^{-6}$ from this value. The solution is unstable.

Figure 3.1: Behavior of the solution for the hydrogen atom for small separations.

4 The heavy hybrid meson spectrum

4.1 Quantum numbers

Mesons are characterized by quantum numbers J^{PC}. Here, J is the total angular momentum of the system, P is the parity and C stands for the behavior under charge conjugation. In comparison, the hybrid static potentials are characterized by different quantum numbers, namely Λ_η^ϵ. To find the quantum numbers of hybrid mesons similar to conventional quark-antiquark bound states, we have to associate the known properties with those quantum numbers.

First of all, we neglected spin in the whole derivation of hybrid meson masses. The two quark spins of 1/2, respectively, can couple to either 0 or 1. Therefore, heavy quark spin multiplets are obtained which are degenerate according to their masses. The eigenstates of the orbital angular momentum operator $\mathbf{L}$ and spin operator $\mathbf{S}$ can be combined to eigenstates of the total angular momentum operator for the system $\mathbf{J}$ using the Clebsch-Gordon-coefficients, $\langle Lm_L; Sm_S|Jm_J\rangle$. The possible values of J are restricted to $|L-S| \leq J \leq |L+S|$. The eigenstates as a solution to the Schrödinger equation are also eigenstates to the parity and charge conjugation operators. Acting with $\mathbf{P}$ on the spherical harmonics yields a factor of $(-1)^L$. Also taking into account the opposite intrinsic parity of the quark and the antiquark gives finally

$$P = (-1)^{L+1}. \tag{4.1}$$

The operator $\mathbf{C}$ acting on the state $\psi = R(r)Y_{Lm}(\theta,\phi)\chi(\vec{S})$ interchanges quark and antiquark, which yields a factor of $(-1)^{L+1}$ with the same arguments as used for parity. Additionally, the charge conjugation flips the spins, this results in a factor of $(-1)^{S+1}$. Combining these factors yields

$$C = (-1)^{L+S} \tag{4.2}$$

as the eigenvalue of charge conjugation [11].

In the case of $\mathbf{A}$, we insert the orbital angular momentum of the quark-antiquark pair $L_{q\bar{q}}$ into the Schrödinger equation. In order to obtain hybrid meson quantum numbers we need the J^{PC}-representation of the gluons. As mentioned before, the potentials obtained from lattice calculations are given in a different representation. There is no simple way to change over to the J^{PC}-representation.

According to [5], the quantum numbers of the gluon can be assigned to 1^{+-} for the two lowest hybrid static potentials Π_u and Σ_u^-. The quantum numbers for quarks and gluon could be added quantummechanically following the *constituent gluon picture*. In this model, the excited gluon field is interpreted as a constituent particle bound to the quark-antiquark pair with quantum numbers in the meson representation.

However, we will label the calculated energies by quantum numbers of the potential, the principal quantum number n and the orbital angular momentum $L_{q\bar{q}}$.

For the case of $\mathbf{B}$, we work in the *Born-Oppenheimer picture*. Here, we associate our results for binding energies with the orbital angular momentum of quarks and total angular momentum of the excited gluon field, $\mathbf{L} = \mathbf{L}_{q\bar{q}} + \mathbf{J}_{gluon}$. The total angular momentum quantum number J for the hybrid meson is derived by adding quantummechanically the spin to the quantum number L. Furthermore, the eigenvalues of parity and charge conjugation for the hybrid meson have to be found. The energy levels derived by solving the Schrödinger equation

Λ_η^ϵ	L	J^{PC} $S=0$	J^{PC} $S=1$	multiplet
Σ_u^-	0	0^{++}	1^{+-}	H_3
	1	1^{--}	$\{0,\mathbf{1},2\}^{-+}$	H_1
	2	2^{++}	$\{1,\mathbf{2},3\}^{+-}$	H_4
Π_u^-	1	1^{++}	$\{\mathbf{0},1,\mathbf{2}\}^{+-}$	H_2
	2	2^{--}	$\{\mathbf{1},2,\mathbf{3}\}^{-+}$	H_5
Π_u^+	1	1^{--}	$\{0,\mathbf{1},2\}^{-+}$	H_1
	2	2^{++}	$\{1,\mathbf{2},3\}^{+-}$	H_4

Table 4.1: J^{PC} quantum numbers from Born-Oppenheimer picture.

can be written as [5]

$$|nLm_L Sm_S;\Lambda\ \eta\ \epsilon\rangle = \int d^3r R_{nL}(r) Y_{Lm_L}(\vec{r})\,|\Lambda\ \eta\ \epsilon;\vec{r}\rangle\,|Sm_S\rangle\,. \tag{4.3}$$

The parity of the gluon field is $\mathbf{P}\,|\Lambda\ \eta\ \epsilon;\vec{r}\rangle = \epsilon(-1)^\Lambda\,|\Lambda\ \eta\ \epsilon;\vec{r}\rangle$. The remaining quark part gives, as before, a factor of $(-1)^{L+1}$. Consequently, the parity of the hybrid meson is given by

$$P = (-1)^{L+\Lambda+1}. \tag{4.4}$$

From the Λ_η^ϵ representation we know the gluon behavior under the combination of parity and charge conjugation which is given by the value of η. As a result, the additional factor to the behavior under charge conjugation of the meson is given by $C = \eta\epsilon(-1)^\Lambda$. Therefore, the eigenvalue of the hybrid meson with respect to charge conjugation is

$$C = \eta\epsilon(-1)^{L+S+\Lambda}. \tag{4.5}$$

The possible quantum numbers resulting from the Born-Oppenheimer picture are given in Table 4.1 where exotic quantum numbers that cannot be obtained in a conventional quark-antiquark picture are printed with bold letters. The multiplets corresponding to Π_u^- and Π_u^+ have the same masses because there exists no difference among their eigenvalue equations. We label the heavy quark spin multiplets in the same way as it is done in [4].

4.2 Probability density

Having a look at the extension of the probability density can serve as a check for the reliability of the calculated energy levels. The probability density to find the quark-antiquark pair with a separation distance r is given by

$$\rho(r) = \int d\Omega|\psi_{nlm}|^2 = \int_0^{2\pi}\int_0^{\pi} |R_{nl}|^2|Y_{lm}|^2 r^2 d\phi sin\theta d\theta = r^2|R_{nl}|^2 = |u_{nl}|^2, \tag{4.6}$$

where we used the normalization of the spherical harmonics and the definition $u_{nl} = rR_{nl}$. The probability densities for different states with principal and orbital angular momentum quantum numbers nl are shown in Figure 4.1. Only radial excitations n should be taken into account for which the probability density does not exceed the region in which the potential parametrisation can be considered valid. The parametrisation can be assumed to describe the

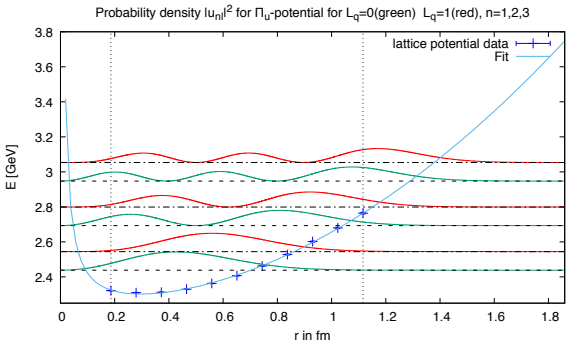

(a) **A**: Π_u for $L_{q\bar{q}} = 0$ (green), $L_{q\bar{q}} = 1$ (red).

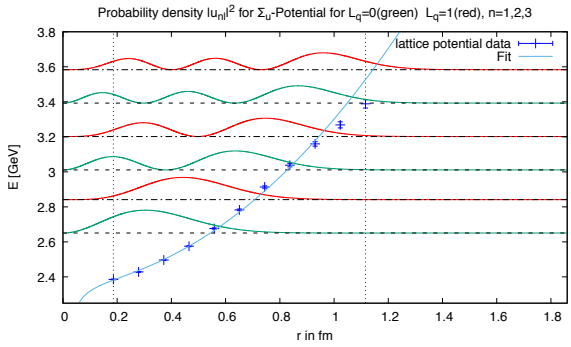

(b) **A**: Σ_u^- for $L_{q\bar{q}} = 0$ (green), $L_{q\bar{q}} = 1$ (red).

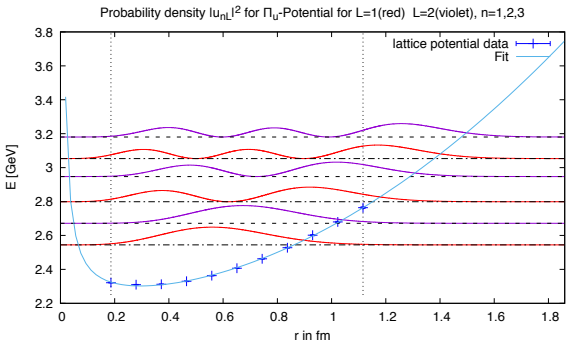

(c) **B**: Π_u for $L = 1$ (red), $L = 2$ (violet).

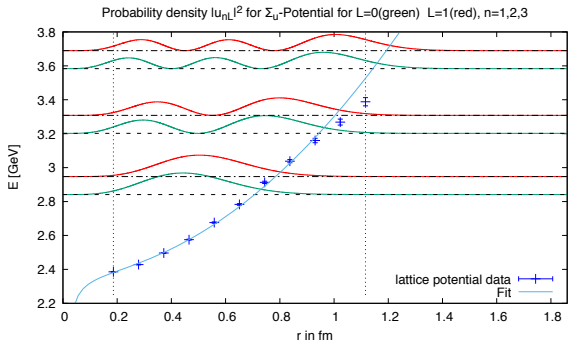

(d) **B**: Σ_u^- for $L = 0$ (green), $L = 1$ (red).

Figure 4.1: Probability density $|u_{nl}|^2$ for both potentials.

data well in the whole region up to quark-antiquark distances of about 1 fm. Therefore, we can regard the two lowest radial excitations $n = 1, 2$ for both potentials, Π_u and Σ_u^-. The probability density is small for separations greater than the upper boundary as displayed by Figure 4.1. Care must be taken in considering results beyond the second excitation.

4.3 Masses

From solving the Schrödinger equation we obtain energy values corresponding to the binding energy E_{nl} for the heavy hybrid meson. The calculated absolute values have no meaning since they are shifted by a constant related to the self energy of the static quarks in lattice calculations. The position of the heavy quarks on the lattice are localized up to the lattice spacing a. Conversely, this implies that the quark momenta are very large and their energy is proportional to $\propto 1/a$. The contribution coming from the infinitely heavy quarks is added to all potentials calculated on the lattice. As a result, a potential computed on a lattice with small lattice spacing a, is shifted upwards in comparison to a potential generated using a larger a. To acquire comparable values for binding energies, there are several options.

The first and easiest method is to take the difference to the lowest bound state, consequently we can compare energy differences that are independent from the energy shift. A main drawback of this method is loosing one state, the lowest one, about which no further statement can be made.

An alternative way to gain comparable results, consists of calculating a simple bound state of two quarks using the same lattice setup and compare the calculated mass to experimental data. A good choice here is the $b\bar{b}$ meson $\eta_b(1S)$ with quantum numbers $J^P = 0^-$. Thus, one can add the energy difference between the higher lying states and the $1S$ state to the experimental mass $m_{exp}(\eta_b(1S))$ like it was done in [1].

The third option, used in the following, is to calculate the energy of the ground state static potential Σ_g^+ at the point of *stringbreaking* and identify this energy with the mass of two B-mesons. At some distance r_{sb} between the two quarks the energy contained in the string between them is sufficient to form two B-mesons from the quark-antiquark meson. B-mesons consist of a heavy antiquark/quark and a light quark/antiquark. So, we identify the value of the potential at the point of stringbreaking, $V_{\Sigma_g^+}(r_{sb})$, with the experimental mass of two B-mesons, $2 * m_{\text{exp}}(B)$.

The stringbreaking distance is calculated from $r_{sb} = (2.27 \pm 0.20) r_0$ [12], using the Sommer parameter r_0. The ground state static potential is

$$\hat{V}_{\Sigma_g^+}(\hat{r}_{sb}) = \hat{V}_0 + \frac{\hat{\alpha}}{\hat{r}_{sb}} + \hat{\sigma}\hat{r}_{sb}, \tag{4.7}$$

with [13]

$$\hat{V}_0 = 0.149 \pm 0.006, \quad \hat{\alpha} = 0.26 \pm 0.02, \quad \hat{\sigma} = 0.0480 \pm 0.0007, \quad \hat{r}_0 = 5.39 \pm 0.02. \tag{4.8}$$

Finally, the computed binding energies E_{nL} for bound states of two bottom quarks with masses $m_{\text{b}}^{(\bar{\text{MS}})} = 4.18$ GeV and an excited gluon field with quantum numbers Π_u and Σ_u^- are presented in Table 4.2.

By adding the difference of binding energies E_{nL} and $V_{\Sigma_g^+}(r_{sb})$ to the mass of two B-mesons we obtain the results for heavy hybrid meson masses independent of the energy shift related to the quark self energy

$$M_{nL} = (E_{nL} - V_{\Sigma_g^+}(r_{sb})) + 10.56 \text{ GeV}. \tag{4.9}$$

The heavy hybrid meson masses are presented in Table 4.3 for the case of **A**, for **B** they are given in Table 4.4. For a graphical presentation, Figures 4.2 and 4.3 show the results in an energy level diagram for case **A** and **B**, respectively.

The errors are the results of a jackknife analysis according to Section 1.2.1, so they only take into account statistical uncertainties.

The results from the Π_u-potential are the same for the naive appraoch **A** and the superior case **B** besides the non-existence of a S-state for **B** as was outlined before. In contrast to this, the Σ_u^--potential differs in an additional term in the centrifugal term for the two cases which results in the fact that masses lie higher in the case of **B**.

To draw a comparison of our results to others, for instance discussed in [4], we would have to adjust the energy offset for the calculated masses or compare mass differences. This is due to the fact that different methods for substraction of the quark self energy are used. Furthermore, the given uncertainties reveal only statistical errors but give no clue to the size of systematic errors in, for example, the quark mass or the choice of parametrisation. However, results so far are encouraging to gain precise heavy hybrid meson masses by applying the presented methods and mentioned enhancements.

	A			**B**		
n	$L_{q\bar{q}}$	Π_u	Σ_u^-	L	Π_u	Σ_u^-
1	0	1.765 ± 0.003	1.964 ± 0.005	0	- -	2.160 ± 0.006
2		2.015 ± 0.005	2.339 ± 0.009		- -	2.531 ± 0.011
1	1	1.874 ± 0.004	2.160 ± 0.006	1	1.874 ± 0.004	2.266 ± 0.007
2		2.129 ± 0.006	2.531 ± 0.011		2.129 ± 0.006	2.637 ± 0.012
1	2	1.995 ± 0.004	2.348 ± 0.008	2	1.995 ± 0.004	2.418 ± 0.009
2		2.252 ± 0.007	2.719 ± 0.014		2.252 ± 0.007	2.788 ± 0.015

Table 4.2: The binding energy values E_{nL} for both potentials in GeV.

$\Lambda_\eta^\epsilon(nL_{q\bar{q}})$	M_{nL}
$\Pi_u(1S)$	10.808 ± 0.003
$\Pi_u(2S)$	11.058 ± 0.005
$\Pi_u(1P)$	10.917 ± 0.004
$\Pi_u(2P)$	11.172 ± 0.006
$\Pi_u(1D)$	11.038 ± 0.004
$\Pi_u(2D)$	11.295 ± 0.007
$\Sigma_u^-(1S)$	11.007 ± 0.005
$\Sigma_u^-(2S)$	11.382 ± 0.009
$\Sigma_u^-(1P)$	11.202 ± 0.006
$\Sigma_u^-(2P)$	11.574 ± 0.010
$\Sigma_u^-(1D)$	11.391 ± 0.008
$\Sigma_u^-(2D)$	11.762 ± 0.014

Table 4.3: **A**: Masses in GeV from hybrid static potentials $\Lambda_\eta^\epsilon(nL_{q\bar{q}})$ for $n = 1, 2$ and $L_{q\bar{q}} = 0, 1, 2 = S, P, D$.

	L	multiplet	J^{PC}	M_{1L}	M_{2L}
Π_u	1	H_2	$\{1^{++}, (0,1,2)^{+-}\}$	10.917 ± 0.003	11.172 ± 0.006
		H_1	$\{1^{--}, (0,1,2)^{-+}, \}$		
	2	H_5	$\{2^{--}, (1,2,3)^{-+}\}$	11.038 ± 0.004	11.295 ± 0.007
		H_4	$\{2^{++}, (1,2,3)^{+-}\}$		
Σ_u^-	0	H_3	$\{0^{++}, 1^{+-}\}$	11.203 ± 0.006	11.574 ± 0.011
	1	H_1	$\{1^{--}, (0,1,2)^{-+}\}$	11.309 ± 0.007	11.680 ± 0.012
	2	H_4	$\{2^{++}, (1,2,3)^{+-}\}$	11.461 ± 0.009	11.831 ± 0.015

Table 4.4: **B**: Masses in GeV from hybrid static potentials for the ground state and first excitations $n = 1, 2$ associated to heavy quark spin multiplets with possible quantum numbers J^{PC}.

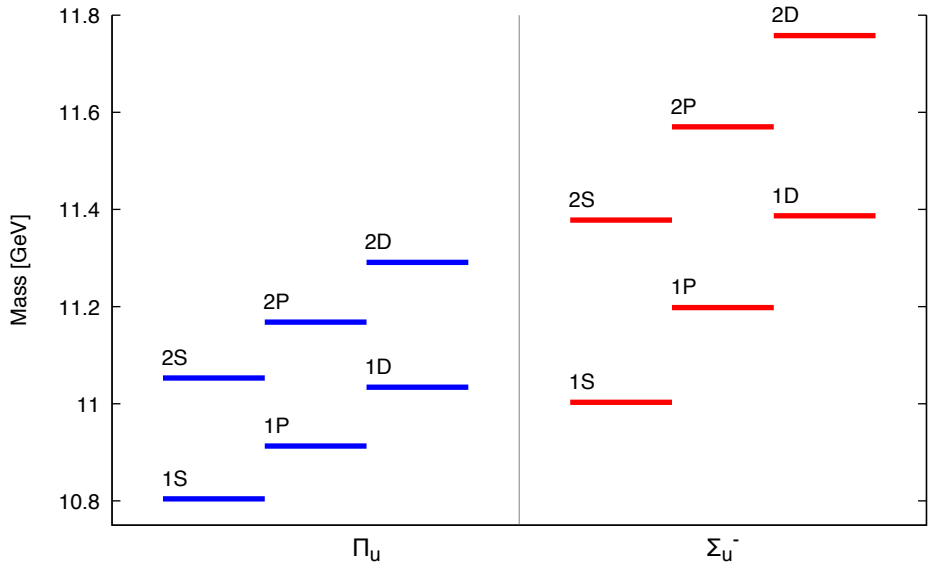

Figure 4.2: **A**: Masses calculated with potentials Λ_η^ϵ with the centrifugal term (**A**).

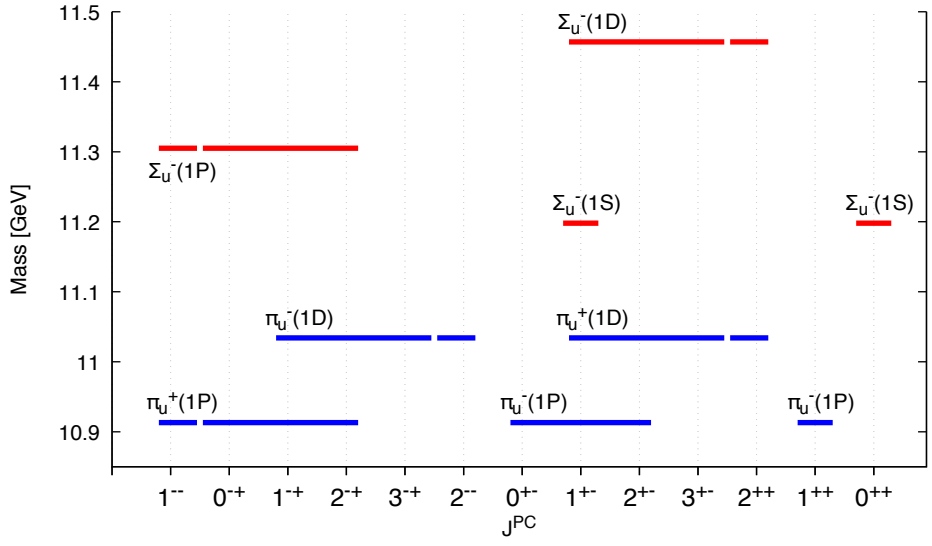

Figure 4.3: **B**: Masses calculated with $\Lambda_\eta^\epsilon(nL)$ associated with quantum numbers J^{PC} .

5 Conclusion and Outlook

In this work, different parametrisations were fitted to lattice data of the hybrid static potentials Π_u and Σ_u^-. Due to the available range of lattice data, the three-parameter-function (2.2) was chosen to fit the whole region from 0.186 fm to 1.116 fm for both hybrid potentials. By means of the Born-Oppenheimer approximation and after evaluating the centrifugal term, we arrived at a one-dimensional, non-relativistic Schrödinger equation for the heavy quark-antiquark pair in a hybrid static potential. The numerical method used to solve the Schrödinger equation for its energy eigenvalues was discussed and tested for the hydrogen atom. After that, we deduced the possible quantum number multiplets for heavy hybrid mesons from the quantum numbers of hybrid static potentials. Finally, the computed masses for a bottom quark-antiquark pair in a hybrid static potential associated with those quantum numbers were presented. The reliability of the calculated spectrum was checked investigating the radial probability density.

In the future, further enhancement can be made to gain an even better understanding of hybrid mesons. As mentioned in Chapter 2, there are different parametrisations. Fits should be improved by combining the functions for small quark-antiquark separations to the one for large r or by fitting potential differences like it was proposed for the Σ_u^--potential. As pointed out before, lattice data for smaller as well as larger interquark distances are required. Subsequently, the developed methods can be perfomed with higher lying hybrid static potentials. Further investigations are needed to improve the estimated uncertainties to take into account not only statistical but also systematic errors. After that, another future aim is to include spin effects in the theoretical treatment that will break the degeneracy between the heavy quark spin multiplets.

References

[1] Michelle Weber. The bottomonium spectrum from the static potential. Master's thesis, Institut für Theoretische Physik, Goethe-Universität Frankfurt am Main, März 2017.

[2] Christian Reisinger. Hybrid static potentials in su(3) gauge theory on the lattice. Master's thesis, Institut für Theoretische Physik, Goethe-Universität Frankfurt am Main, März 2017.

[3] http://www.physics.utah.edu/ detar/phycs6730/handouts/jackknife/jackknife/, 2017.

[4] Matthias Berwein, Nora Brambilla, Jaume Tarrús Castellà, and Antonio Vairo. Quarkonium Hybrids with Nonrelativistic Effective Field Theories. *Phys. Rev.*, D92(11):114019, 2015.

[5] Eric Braaten, Christian Langmack, and D. Hudson Smith. Born-Oppenheimer Approximation for the XYZ Mesons. *Phys. Rev.*, D90(1):014044, 2014.

[6] GSL Project. GSL - GNU scientific library. http://www.gnu.org/software/gsl/, 2017.

[7] Antonio Vairo. Quarkonia: a theoretical frame. In *3rd International Workshop on Charm Physics (Charm 2009) Leimen, Germany, May 20-22, 2009*, 2009.

[8] K. Jimmy Juge, Julius Kuti, and Colin Morningstar. Fine structure of the QCD string spectrum. *Phys. Rev. Lett.*, 90:161601, 2003.

[9] K. J. Juge, J. Kuti, and C. J. Morningstar. Ab initio study of hybrid anti-b g b mesons. *Phys. Rev. Lett.*, 82:4400–4403, 1999.

[10] Nora Brambilla, Gastão Krein, Jaume Tarrús Castellà, and Antonio Vairo. The Born-Oppenheimer approximation in an effective field theory language. 2017.

[11] Curtis A. Meyer. Light and exotic mesons. http://www.curtismeyer.com/material/lecture.pdf.

[12] SESAM Collaboration. Observation of string breaking in qcd. *Phys.Rev.D71:114513*, 2005.

[13] Christian Reisinger. unpublished notes. June 2017.

[14] Philipp Wolf and Marc Wagner. Lattice study of hybrid static potentials. *J. Phys. Conf. Ser.*, 599(1):012005, 2015.

[15] Norbert Straumann. *Quantenmechanik - Ein Grundkurs über nichtrelativistische Quantentheorie*. Springer-Verlag, Berlin Heidelberg New York, 2013.

A Behavior of the radial wave function for $r \to 0$

The behavior of the radial wave function for large r is easily determined by considering the following. Since the total wave function is required to be normalised, the radial probability amplitude has to fulfill the normalization condition

$$\int_0^\infty |u_{nl}|^2 dr = 1. \tag{A.1}$$

According to this, the radial probability amplitude $u_{nl}(r) = rR(r)$ has to vanish for $r \to \infty$.

Now, we investigate the behavior of u_{nl} for $r \to 0$. The hybrid static potential in the form of Equation (2.2) is inserted into the radial Schrödinger equation

$$\left(\frac{-1}{2\mu} \left[\frac{\partial^2}{\partial r^2} + \frac{2}{r} \frac{\partial}{\partial r} \right] + \frac{\left\langle \mathbf{L}^2_{q\bar{q}} \right\rangle^{(m)}}{2\mu r^2} + V_m(r) - E^{(m)}_{nl} \right) R(r) = 0. \tag{A.2}$$

This is an ordinary differential equation with singularities at $r = 0$. For finding the appropriate boundary condition for the radial wave function it is useful to choose the following ansatz [15]

$$R(r) = r^s \sum_{k=0}^{\infty} a_k r^k,\ a_0 \neq 0. \tag{A.3}$$

The term in the parametrisation (2.2) proportional to $\propto r^2$ is only dominant for large r, thus can be neglected in the region of small separations. Inserting the ansatz into Equation (A.2) yields

$$\begin{aligned} -\frac{1}{2\mu} \left[s(s-1) r^{s-2} \sum_0^\infty a_k r^k + s r^{s-1} \sum_0^\infty k a_k r^{k-1} + s r^{s-1} \sum_0^\infty k a_k r^{k-1} + r^s \sum_0^\infty k(k-1) a_k r^{k-2} \right] \\ - \frac{1}{\mu} \left[s r^{s-2} \sum_0^\infty a_k r^k + r^{s-1} \sum_0^\infty k a_k r^{k-1} \right] \\ + \frac{\left\langle \mathbf{L}^2_{q\bar{q}} \right\rangle^{(m)}}{2\mu} r^{s-2} \sum_0^\infty a_k r^k + r^s (c_1 - E) \sum_0^\infty a_k r^k + r^{s-1} c_2 \sum_0^\infty a_k r^k \\ = 0 \end{aligned} \tag{A.4}$$

With the relations $\sum_{k=0}^\infty k a_k r^{k-1} = \sum_{k=0}^\infty a_{k+1} r^k$ and $\sum_{k=2}^\infty a_k r^{k-2} = \sum_{k=0}^\infty a_{k+2} r^k$ the terms

are sorted with respect to their power in r:

$$\begin{aligned} & r^{s-2}\left[\left(-\frac{s(s-1)}{2\mu}-\frac{s}{\mu}+\frac{\left\langle \mathbf{L}_{q\bar{q}}^2\right\rangle^{(m)}}{2\mu}\right)a_0\right] \\ & +r^{s-1}\left[\left(-\frac{s(s-1)}{2\mu}-\frac{2(2s-1)}{2\mu}+\frac{\left\langle \mathbf{L}_{q\bar{q}}^2\right\rangle^{(m)}}{2\mu}\right)a_1+c_2\ a_0\right] \\ & +r^s\sum_k\left[\frac{-1}{2\mu}\left((s+k+3)(s+k+2)-\left\langle \mathbf{L}_{q\bar{q}}^2\right\rangle^{(m)}\right)a_{k+2}+c_2\ a_{k+1}+(c_1-E)\,a_k\right]r^k \\ & = 0. \end{aligned} \tag{A.5}$$

All three terms have to vanish separately so that this equation is fulfilled. From this, a conditional equation for s follows:

$$s(s+1)-\left\langle \mathbf{L}_{q\bar{q}}^2\right\rangle^{(m)}=0 \tag{A.6}$$

Now we distinguish the cases of different centrifugal terms:

- **A**: For $\left\langle \mathbf{L}_{q\bar{q}}^2\right\rangle^{(m)} = L_{q\bar{q}}(L_{q\bar{q}}+1)$ the value of s is either $L_{q\bar{q}}$ or $-(L_{q\bar{q}}+1)$. The latter option would imply an unbounded wave function so that we choose $s = L_{q\bar{q}}$. For the radial probability amplitude follows the boundary condition

$$r \to 0 : u_{nl}(r) \sim r^{L_{q\bar{q}}+1}. \tag{A.7}$$

- **B**: For the Π_u-potential the centrifugal term looks the same as in **A** besides the quark-antiquark orbital angular momentum is replaced by the orbital angular momentum of the meson. The behavior of the radial probability amplitude for small separations is described by

$$r \to 0 : u_{nl}(r) \sim r^{L+1}. \tag{A.8}$$

  For the Σ_u^--potential we obtain non-integer values for s given by

$$s = \frac{1}{2}(\sqrt{4L^2+4L+9}-1) \tag{A.9}$$

  so that we write

$$r \to 0 : u_{nl}(r) \sim r^{s+1}. \tag{A.10}$$

B Erklärung nach § 30 (12) Ordnung für den Bachelor- und dem Masterstudiengang

Hiermit erkläre ich, dass ich die Arbeit selbstständig und ohne Benutzung anderer als der angegebenen Quellen und Hilfsmittel verfasst habe. Alle Stellen der Arbeit, die wörtlich oder sinngemäß aus Veröffentlichungen oder aus anderen fremden Texten entnommen wurden, sind von mir als solche kenntlich gemacht worden. Ferner erkläre ich, dass die Arbeit nicht - auch nicht auszugsweise - für eine andere Prüfung verwendet wurde.

Frankfurt am Main, den 14. September

(Carolin Riehl)